CHAPTER IV
RESULTS AND DISCUSSION

4.1 Catalyst Characterization

4.1.1 Thermo Gravimetry/Differential Thermal Analyzer (TG-DTA)

The thermal decomposition behavior and the suitable calcinations temperature of the catalysts were studied by using thermogravimetry and differential thermal analysis (TG-DTA). Figure 4.1 (a) and (b) shows TG-DTA curve of dried TiO_2 support systhesized via a combined sol-gel process with surfactant-assisted templating method denoted as SG-TiO_2 and Pd/TiO_2 catalyst synthesized via a combined single-step sol-gel process with surfactant-assisted templating method (SATM) denoted as SSSG. The DTA curve shows two main exothermic regions. The first exothermic peak, with its position between 250 °C and 350 °C, is attributed to the burnout of the surfactant template, including with the removal of organic remnants in case of SSSG catalyst. The second exothermic peak between 350 °C and 500 °C corresponds to the crystallization process of the support and also the removal of organic remnant and chemisorbed water molecule (Hague *et al*, 1994). The difference of two catalysts can be noticed from the crystallization peak that SSSG Pd/TiO_2 released larger extent of heat for crystallization than the SG-TiO_2, indicating the higher thermal stability of the TiO_2 support with Pd loading (Sreethawong *et al.*, 2006). From Figure 4.2 (a) – (d), TG-DTA curves of P25-IWI, P25-PCD, SG-IWI, and SG-PCD Pd/TiO_2 catalyst, respectively, were shown. From TG-DTA results of four catalysts, the first exothermic peak, with its position lower than 150 °C, is attributed to the removal of physisorbed water molecules. The exothermic region between 350 and 500 °C corresponds to the removal of organic remnants and chemisorbed water molecule (Hague *et al.*, 1994).

The TG result reveals that the weight loss ends at a temperature of approximately 500 °C for all catalysts. Hence, the calcination temperature at 500 °C is sufficient for the complete removal of the organic surfactant molecules, organic remnant, and the catalyst crystallization process (Sreethawong *et al.*, 2009).

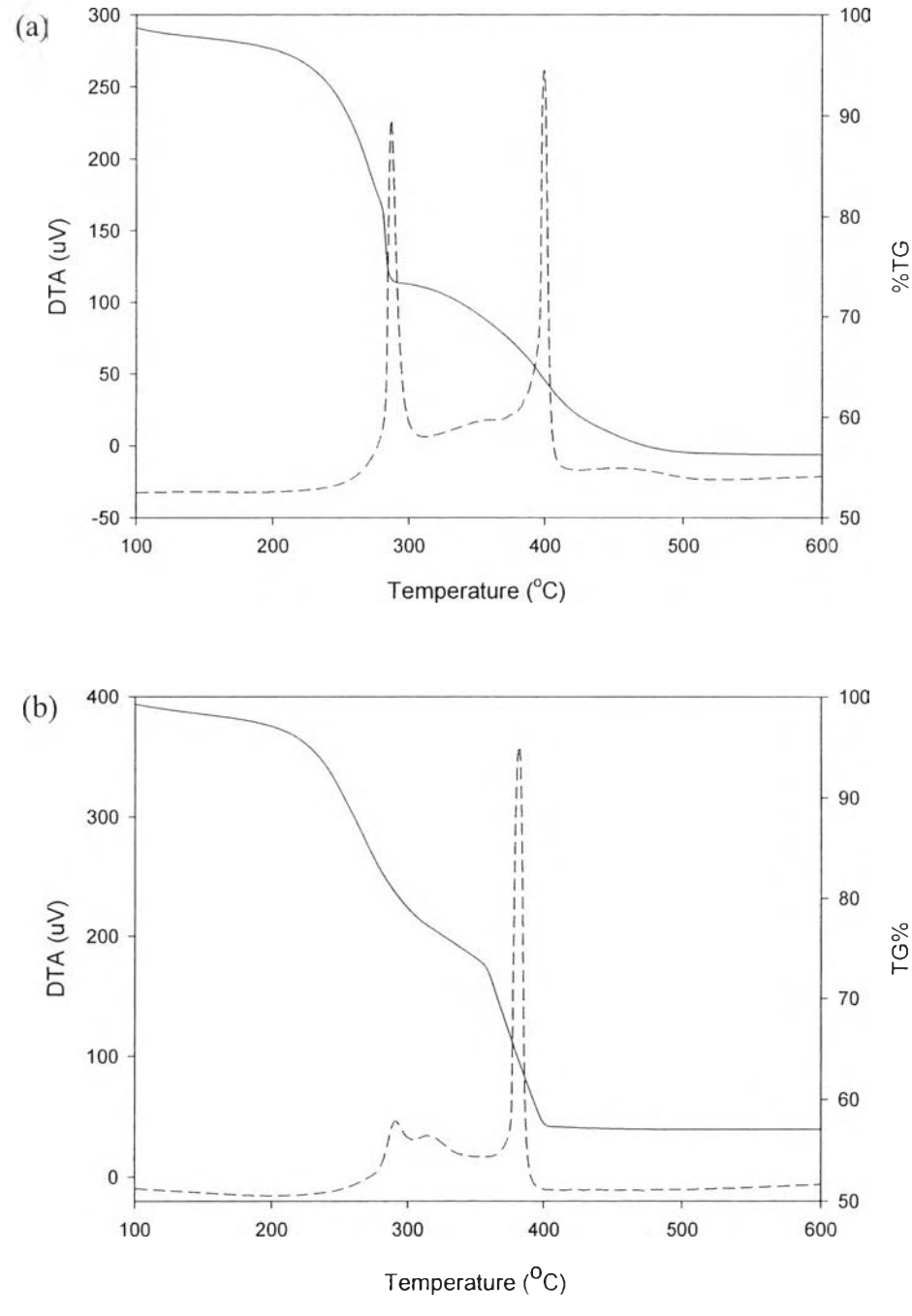

Figure 4.1 TG-DTA curve of dried samples: (a) TiO_2 support synthesized via a combined sol-gel process with SATM (SG-TiO_2) and (b) Pd/TiO_2 catalyst synthesized via a combined single-step sol-gel process with SATM (SSSG).

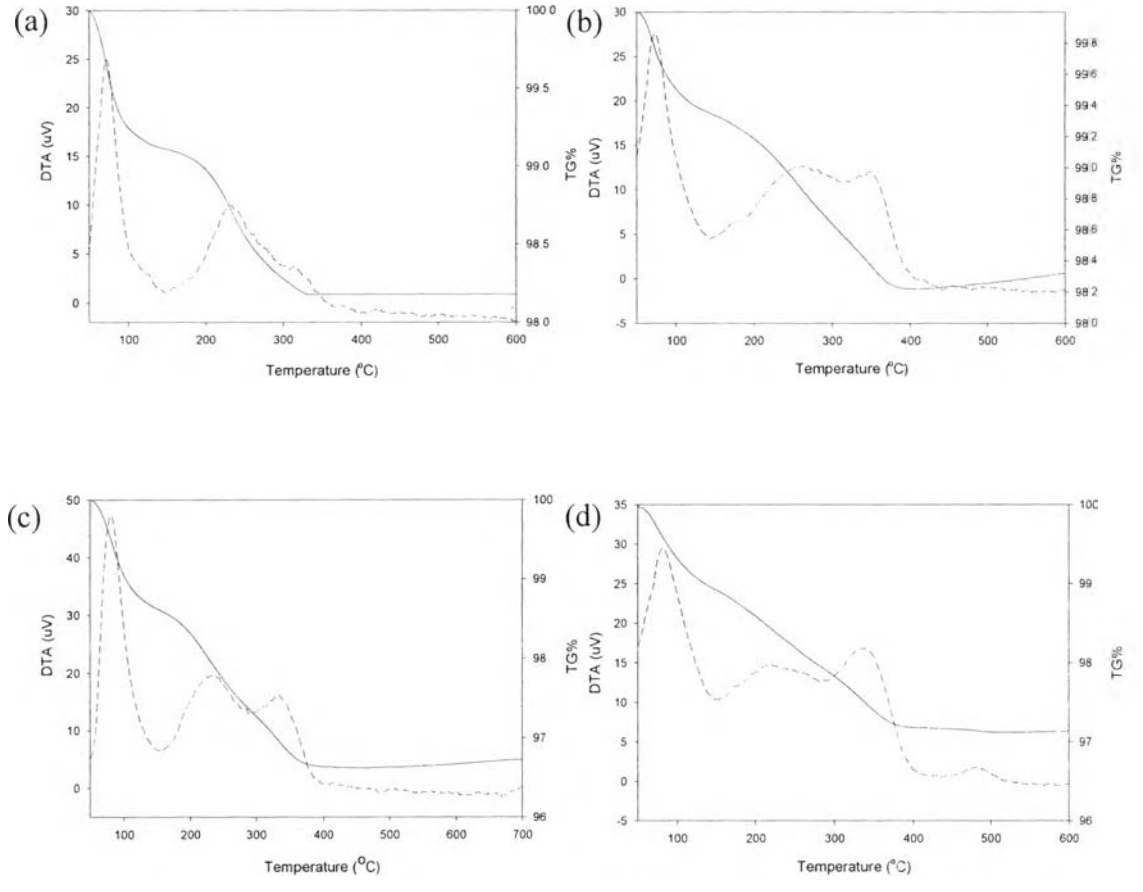

Figure 4.2 TG-DTA curve of Pd/TiO_2 catalyst: (a) P25-IWI, (b) P25-PCD, (c) SG-IWI, and (d) SG-PCD.

4.1.2 N_2 Adsorption-Desorption

N_2 adsorption-desorption analysis was used to investigate the mesoporosity of the catalysts by using the characteristics of the isotherm shape. The adsorption-desorption isotherm of the SG-TiO_2 support reveals the typical IUPAC type IV pattern with the H2 hysteresis loop, which is associated with capillary condensation taking place in mesopores. Besides, the isotherm also shows the limiting uptake over a range of high relative pressure (P/P^0) that is another characteristic feature of a mesoporous material (Sing *et al.*, 1985), as shown in Figure 4.3 (a). With the commercial P-25 TiO_2 support denoted as P25-TiO_2, the absence of both a hysteresis loop and an adsorption plateau at very high relative

pressure indicates that there is no capillary condensation of N_2 into the pore corresponding to the IUPAC type II that possesses the non-mesoporous characteristics, as shown in Figure 4.3 (b) (Sreethawong *et al.*, 2009). The inset of Figure 4.3 (a) and (b) shows the pore size distribution curve calculated from the desorption branch of the isotherm by the BJH method. SG-TiO_2 support exhibited a narrow pore size distribution as shown in Figure 4.3 (a), while, the inset of Figure 4.3 (b) that is the pore size distribution of P25-TiO_2 support is quite broad which is not only present in the mesoporous region (between 2 to 50 nm) but also exist in the macroporous region (> 50 nm).

In case of Pd/TiO_2 catalysts, SG-IWI, SG-PCD and SSSG catalysts exhibited the typical IUPAC type IV pattern with the H2 hysteresis loop that is the mesoporous characteristic, including with the very narrow pore size distribution that present in the mesoporous region as shown in Figure 4.4. On the other hand, P25-IWI and P25-PCD catalyst showed the typical IUPAC type II pattern and the broad pore size distribution which are similar to those of P25-TiO_2 support as shown in Figure 4.5.

The textural properties obtained from the N_2 adsorption-desorption isotherm (i.e., BET surface area, mean pore diameter, and total pore volume) of the catalysts are summarized in Table 4.1. It is clearly seen that the surface area of SG-TiO_2 support was much higher than that of the commercial P25 TiO_2 support, which may contribute to the high activity for the deoxygenation of beef fat for the production of hydrogenated biodiesel. For Pd/TiO_2 catalysts, it is seen that the surface area of loaded catalysts was lower when compared to the unloaded TiO_2 support. On the contrary, SSSG catalyst showed the highest surface area although Pd was loaded on the support. It may result in the higher thermal stability of the TiO_2 support with Pd loading (Sreethawong *et al.*,2006) as observed in TGA result.

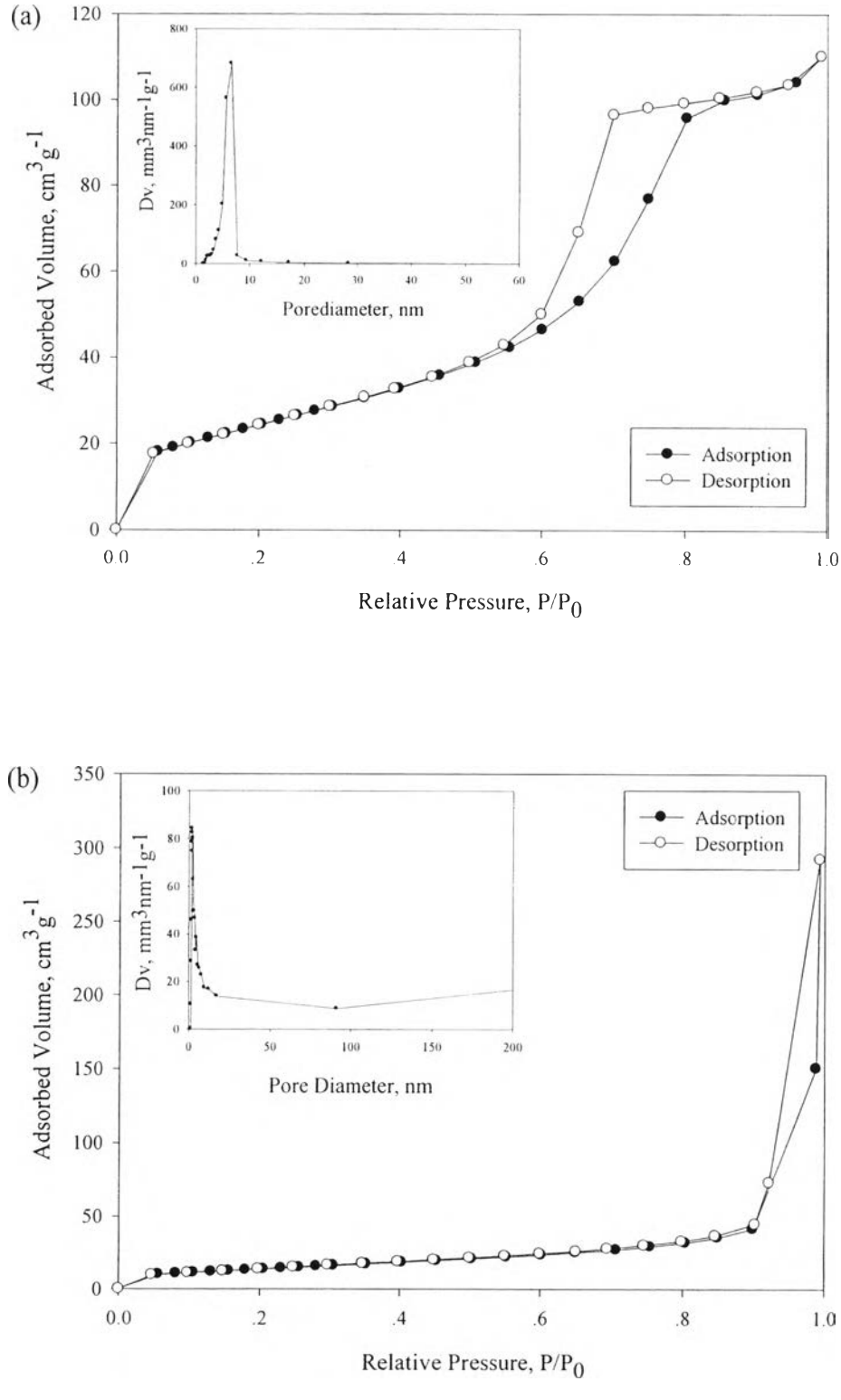

Figure 4.3 N_2 adsorption-desorption isotherm of TiO_2 supports: (a) SG-TiO_2 and (b) P25-TiO_2 (inset: pore size distribution).

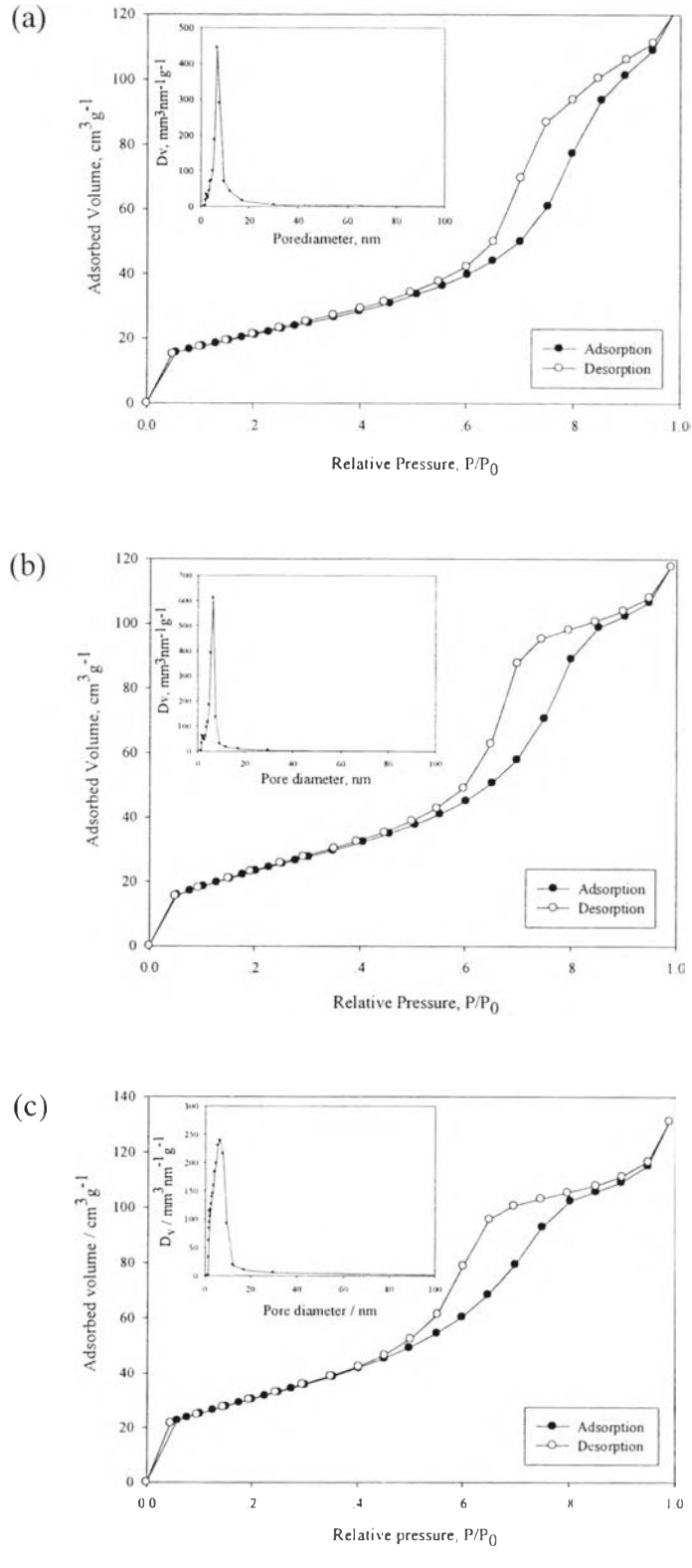

Figure 4.4 N_2 adsorption-desorption isotherm of Pd/TiO_2 catalysts: (a) SG-IWI, (b) SG-PCD, and (c) SSSG (inset: pore size distribution).

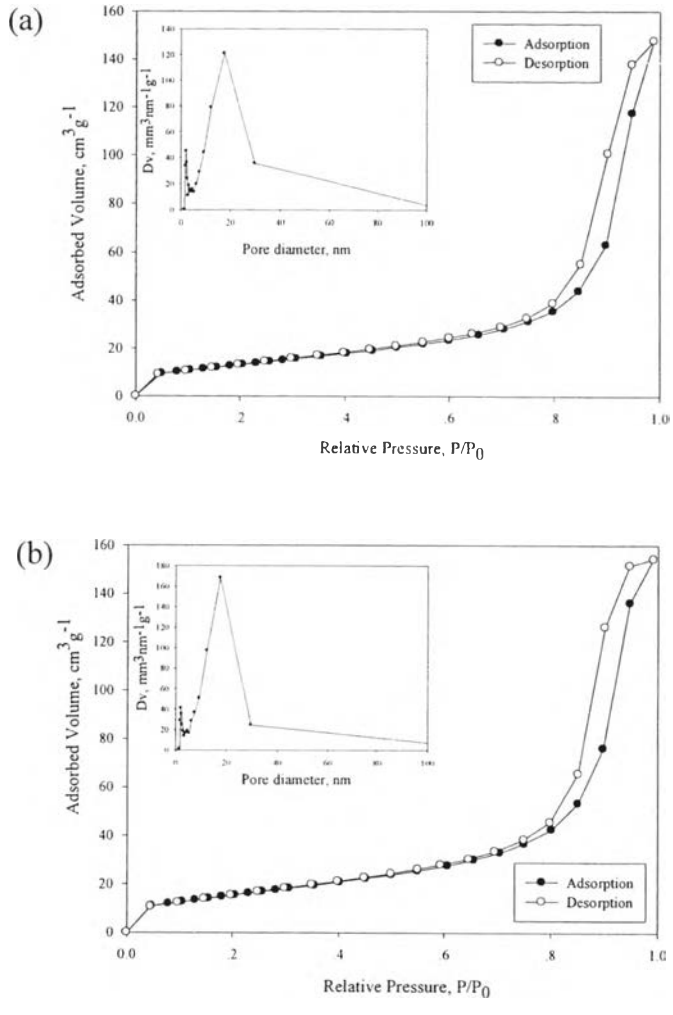

Figure 4.5 N_2 adsorption-desorption isotherm of Pd/TiO_2 catalysts: (a) P25-IWI, and (b) P25-PCD (inset: pore size distribution).

Table 4.1 Textural properties of the catalysts

Catalyst	Surface area (m^2/g)	Total pore volume (cm^3/g)	Mean pore diameter (nm)
SG-TiO_2	89.60	0.170	7.61
P25-TiO_2	50.50	0.230	18.50
P25-IWI	48.80	0.228	18.70
SG-IWI	77.30	0.187	9.66
P25-PCD	49.70	0.239	16.80
SG-PCD	88.20	0.182	8.26
SSSG	113.00	0.203	7.19

4.1.3 X-ray Diffraction (XRD)

XRD analysis, one of the most powerful techniques for identification of crystalline structure, was employed to investigate the crystallinity and purity of prepared samples. The XRD patterns of all catalysts are shown in Figure 4.6. The XRD pattern of the SG-TiO_2 catalyst indicated the crystalline structure of the pure anatase phase owing to dominant peaks at 2θ of 25.2°, 37.9°, 48.3°, 53.8°, 62.7°, 68.9°, and 75.3°, which represent the indices of (101), (103), (200), (105), (213), (116), and (107) planes, respectively. For commercial P-25 TiO_2, the occurance of the peaks at 2θ of about 27.5°, 36.0 °, 41.2°, 44.1°, 54.2°, 56.7°, 64.2°, and 69°, which correspond to the indices of (110), (101), (111), (210), (211), (220), (310), and (301) planes, respectively, indicates that it comprises a mixture of anatase and rutile phases with approximately 78% rutile content that is calculated from XRD intensity data by Spurr and Myers' method as illustrated in the following relationships (Sreethawong *et al.*, 2009).

$$W_R = \left[1 + \frac{0.8I_A}{I_R}\right]^{-1}$$

$$W_A = 1 - W_R$$

Where I_A and I_R represent the integrated intensities of the anatase (101) and rutile (110) diffraction peaks. Not only the phase identification, the crystallite size of the catalysts, estimated from line broadening of anatase (101) and rutile (110) diffraction peaks using Sherrer's equation, is also summarized in Table 4.2. The results revealed that the crystallite size of SG-TiO_2 and Pd supported SG-TiO_2 catalyst is in the range of 13-14 nm. With the P25-TiO_2 and Pd supported P25-TiO_2 catalyst, the crystallite size are in the range of 18-22 nm and 8-12 nm for anatase and rutile phase, respectively.

Nevertheless, the presence of Pd owing to dominant peaks at 40 (Pd (111)), 46.5 (Pd (200)), and 68 (Pd (221)) could not be observed at all of the palladium supported titania catalysts, likely due to the combination of their low content, high degree of dispersion and small particle size (Sreethawong *et al.*, 2005).

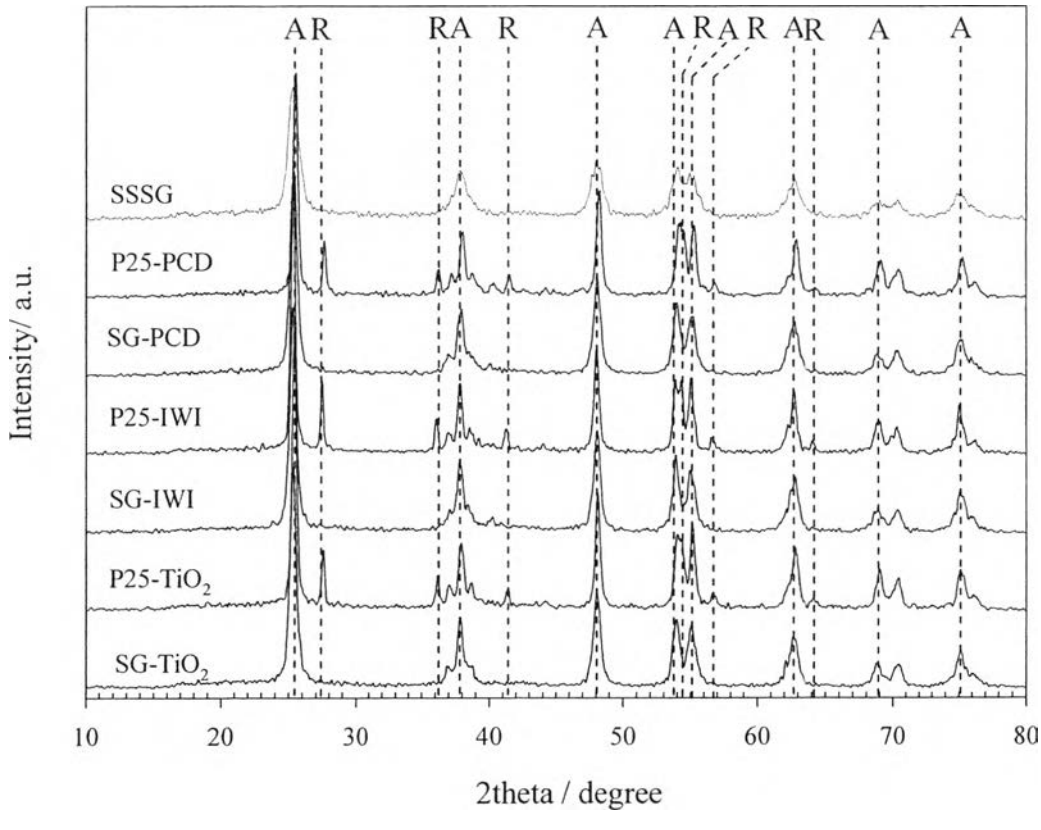

Figure 4.6 XRD patterns of SG-TiO_2, P25-TiO_2, Pd/TiO_2 catalyst: SG-IWI; P25-IWI; SG-PCD; P25-PCD and ;SSSG (A:anatase, R:rutile).

Table 4.2 Summary of XRD analysis of catalysts

Catalyst	Phase from XRD pattern	Rutile ratio (W_R)	Crystallite size (nm)	
			Anatase (101)	Rutile (110)
SG-TiO_2	Anatase	-	14.43	-
P25-TiO_2	Anatase+Rutile	0.22	20.45	8.62
SG-IWI	Anatase	-	14.18	-
P25-IWI	Anatase+Rutile	0.25	21.72	11.96
SG-PCD	Anatase	-	13.02	-
P25-PCD	Anatase+Rutile	0.24	18.80	8.41
SSSG	Anatase	-	8.57	-

4.1.4 Atomic Absorption Spectroscopy (AAS)

Atomic absorption spectroscopy (AAS) is considered as a spectroanalytical technique for the quantitative determination of chemical elements. Therefore, this technique was employed to determine the actual metal loading of the Pd supported TiO_2 catalysts. The AAS results are summarized in Table 4.3. The results revealed the presence of Pd on the TiO_2 support in higher amount by using incipient wetness impregnation method compared with single-step sol-gel method and photochemical deposition method, respectively. The actual metal loading of SSSG catalyst should be close to 1 wt% but it appeared only 0.83 wt%. The lacking of the metal particles may due to good dispersion in the mesopore structure during sol-gel formation which is more difficult to completely digest by aqua regia or nitrohydrochloric acid in 2 h. Moreover, palladium metal particles can be deposited by photochemical deposition method on titania support in low amount. Parameters that may affect the results could be the type of Hg lamp (low, high pressure), duration of irradiation, and palladium precursor.

Table 4.3 The actual metal loading of the catalysts

Catalyst	Actual metal loading (wt%)
SG-IWI	0.92
P25-IWI	0.96
SG-PCD	0.64
P25-PCD	0.73
SSSG	0.83

4.1.5 Hydrogen Chemisorption

The reduced catalysts were characterized to determine the dispersion of Pd on the surface of catalysts. The dispersion was calculated from the amount of H_2 consumed on the Pd surface, assuming the Pd:H stoichiometry to be unity. The results are shown in Table 4.4. SSSG provided the highest Pd dispersion among other Pd/TiO_2 catalysts. Palladium ion may well disperse in mesopore of TiO_2 support during sol-gel process with surfactant-assisted templating method. Furthermore, the higher surface area of support also provides the higher metal dispersion as seen in the difference between palladium loaded on SG-TiO_2 support and that on P25-TiO_2 support. (Bonarowska *et al.*, 2000 and Castellazzi *et al*, 2010)

Table 4.4 The percent metal dispersion of palladium supported titania catalysts

Catalyst	Pd dispersion (%)*
SG-IWI	26.73
P25-IWI	3.61
SG-PCD	13.74
P25-PCD	4.45
SSSG	34.88

*Analyzed by hydrogen chemisorptions at 110 °C assuming the Pd:H stoichiometry to be unity

4.1.6 Temperature-Programmed Oxidation (TPO)

The TPO profiles and amounts of coke deposit of spent catalysts (after 6 TOS) are illustrated in Figure 4.7 and Table 4.5, respectively. For all Pd-supported titania catalysts, the peaks observed at temperatures below 400 °C represented the weakly coke deposit on the support. P25-PCD and P25-IWI catalysts showed the high coke formation of 10.79 and 10.42 wt.%, respectively, whereas SG-IWI, SSSG, and SG-PCD catalyst showed the low coke formation among other Pd/TiO_2 catalysts (7.55, 8.04, and 8.92 wt.%, respectively). The low coke deposit could be due to their high surface area and highly dispersed metal, minimizing the effect of catalyst deactivation caused by sintering and/or coking.

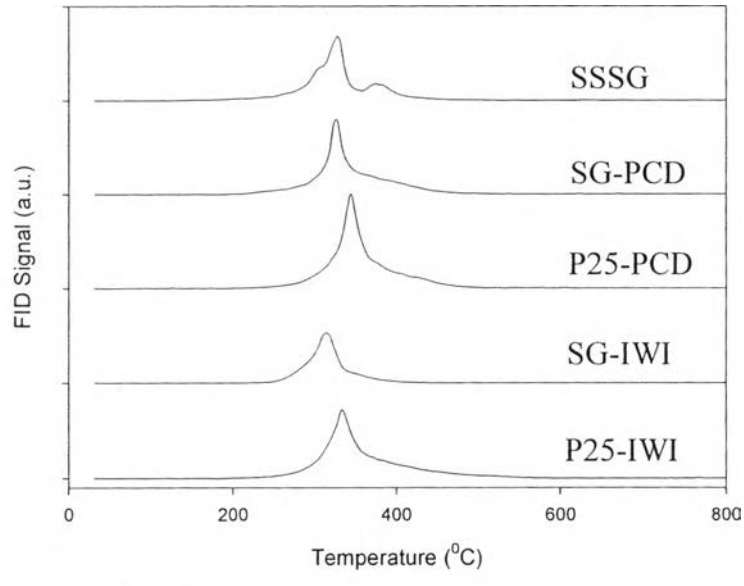

Figure 4.7 TPO profiles of spent catalysts after reaction.

Table 4.5 Amount of carbon deposit on the spent catalyst after reaction

Catalyst	Carbon deposit (wt.%)
SG-IWI	7.55
P25-IWI	10.42
SG-PCD	8.92
P25-PCD	10.79
SSSG	8.04

4.2 Deoxygenation of Beef Fat

4.2.1 Standard Analysis

The chemical standards of products from catalytic activity testing such as dodecane (n-C_{12}), pentadecane (n-C_{15}), hexadecane (n-C_{16}), heptadecane (n-C_{17}), octadecane (n-C_{18}), eicosane (n-C_{20}), hexadecanol, octadecanol, palmitic acid, oleic acid, stearic acid, ester group, monoglyceride group, diglyceride group, and triglyceride group were analyzed by gas chromatograph equipped with an FID detector (Agilent 7890) to identify peaks of compositions of feedstocks, intermediates and products. The chromatograms are shown in Figures 4.8 - 4.13. The retention time and response factor of the standards are shown in Table 4.6.

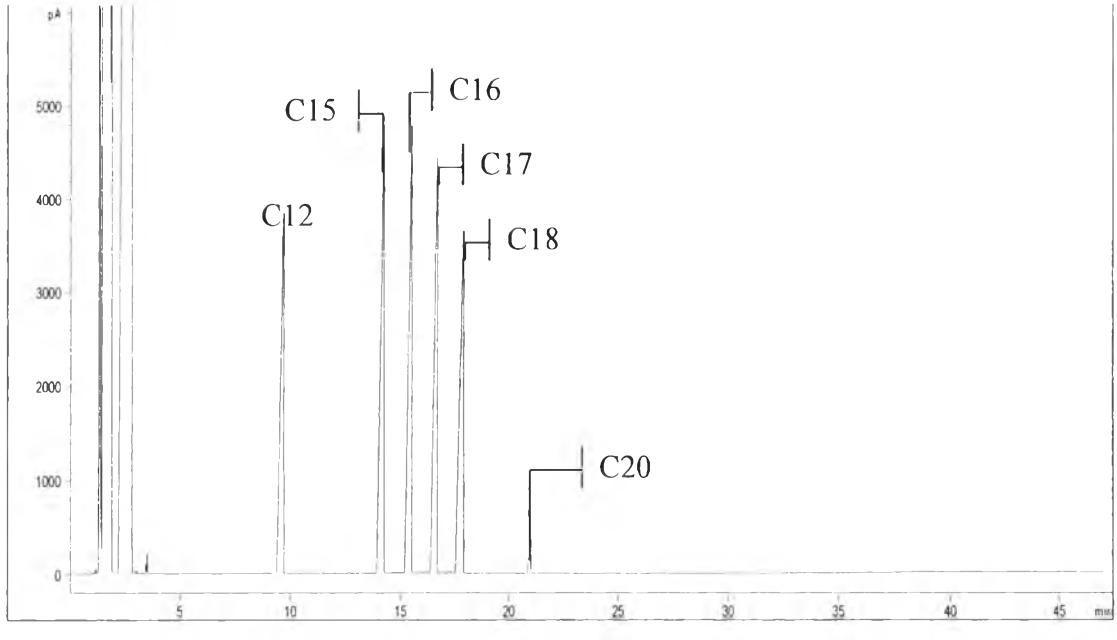

Figure 4.8 Chromatograms of standard n-alkanes: n-pentadecane, n-hexadecane, n-heptadecane, n-octadecane.

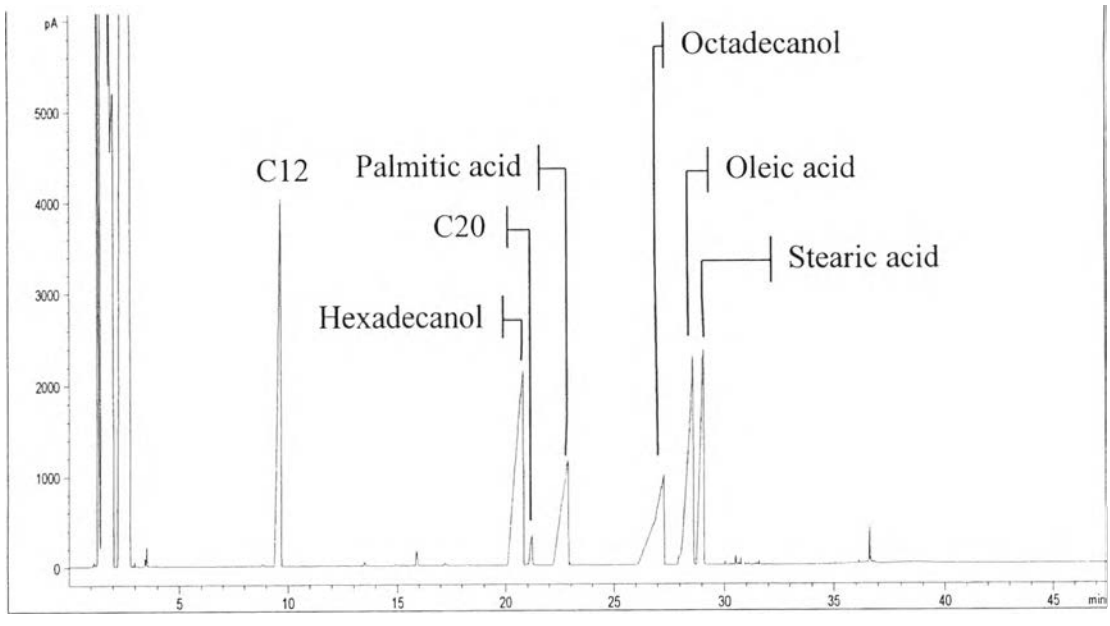

Figure 4.9 Chromatograms of standard fatty alcohols and fatty acids: hexadecanol, octadecanol, palmitic acid, stearic acid, and oleic acid.

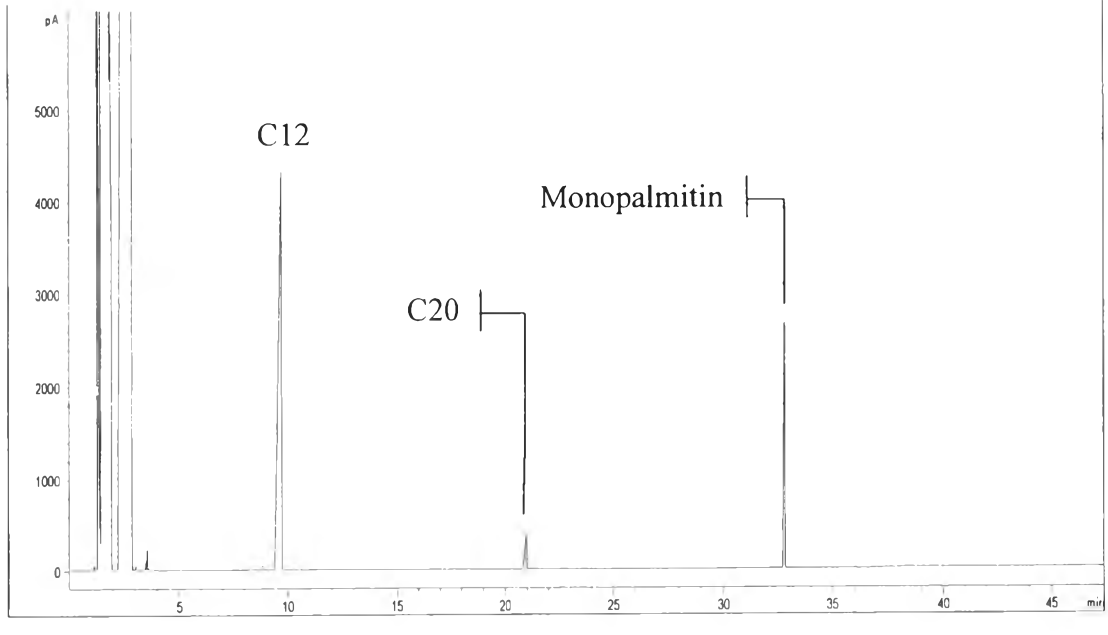

Figure 4.10 Chromatograms of standard monoglyceride: monopalmitin.

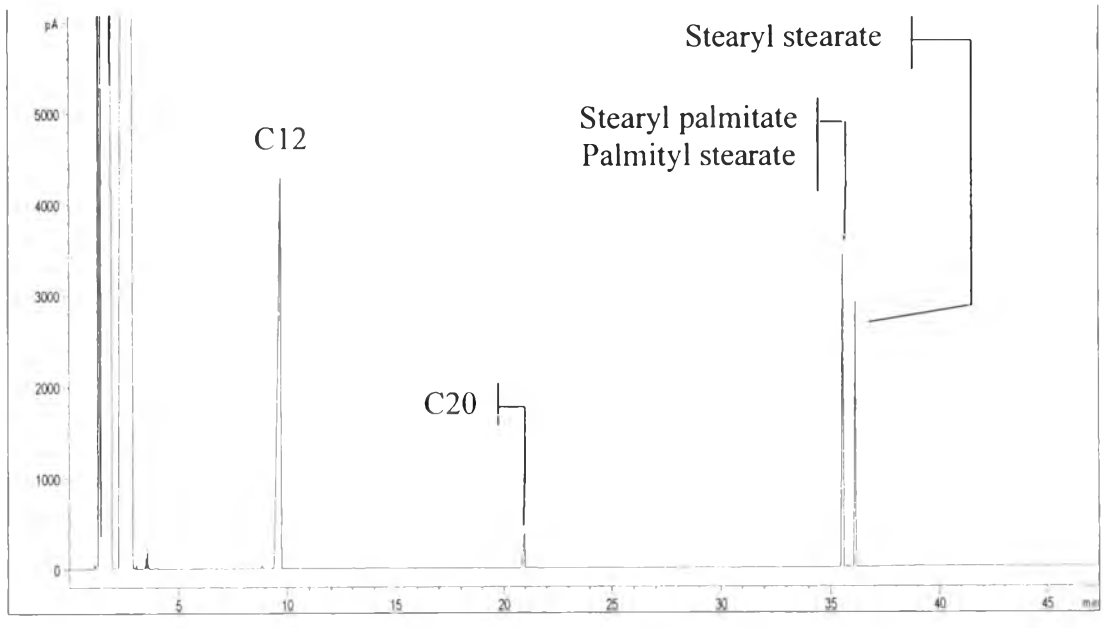

Figure 4.11 Chromatograms of standard fatty esters: stearyl palmitate, palmityl stearate, stearyl stearate.

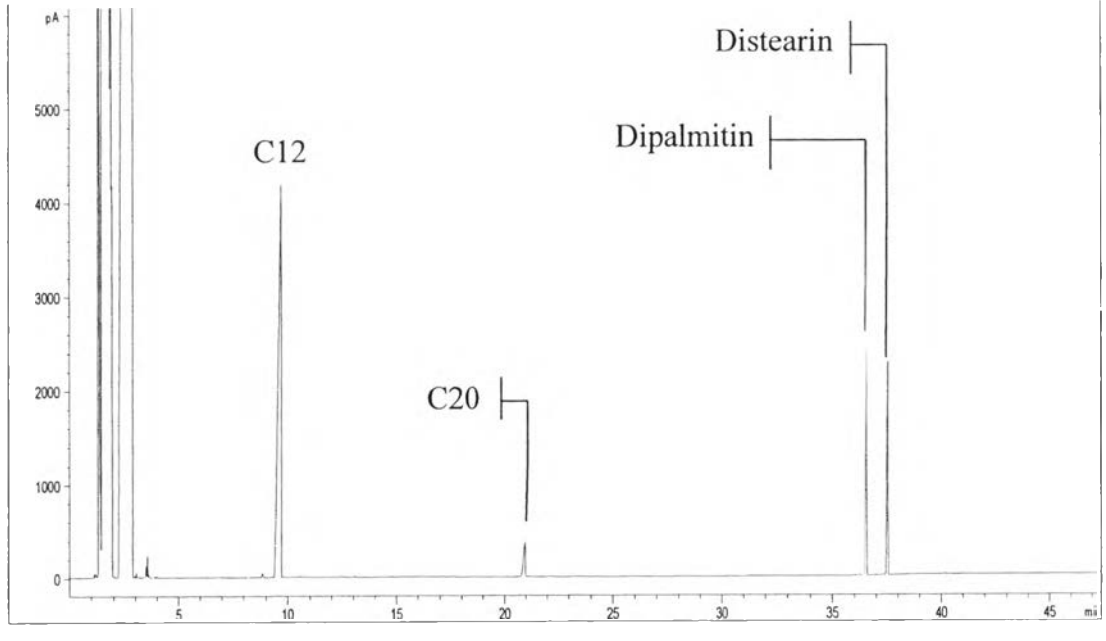

Figure 4.12 Chromatograms of standard diglycerides: dipalmitin and distearin.

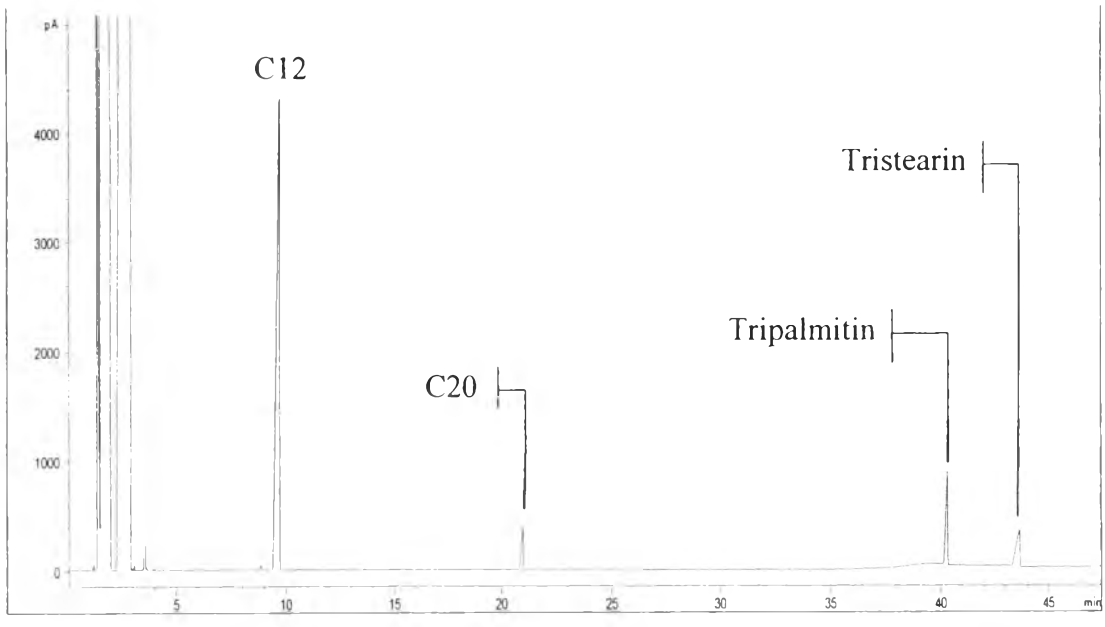

Figure 4.13 Chromatograms of standard triglycerides: tripalmitin and tristearin.

Table 4.6 Retention times and response factors of standard chemicals

Standard chemicals	Retention times	Response factors
n-Pentadecane	14.208	1.034
n-Hexadecane	15.506	1.029
n-Heptadecane	16.679	1.029
n-Octadecane	17.904	1.047
Hexadecanol	20.707	1.092
Octadecanol	27.293	1.078
Palmitic acid	22.878	1.103
Stearic acid	29.082	1.045
Oleic acid	28.600	0.985
Stearyl palmitate	35.562	1.077
Palmityl stearate		0.912
Stearyl stearate	36.132	0.975
Monopalmitin	32.835	1.103
Dipalmitin	36.559	0.972
Distearin	37.558	0.971
Tripalmitin	40.326	0.989
Tristearin	43.685	0.946

4.2.2 Feed Analysis

The 20 vol.% beef oil in dodecane was analyzed with gas chromatograph to identify its components. The gas chromatograph and composition of beef fat as shown in Figure 4.14 and Table 4.7, respectively, reveal that beef oil contain triglyceride as main component with trace amount of free fatty acid (e.g. oleic acid and stearic acid). Besides, the fatty acid composition of beef oil analyzed by AOAC 966.06-GC method is listed in Table 4.8.

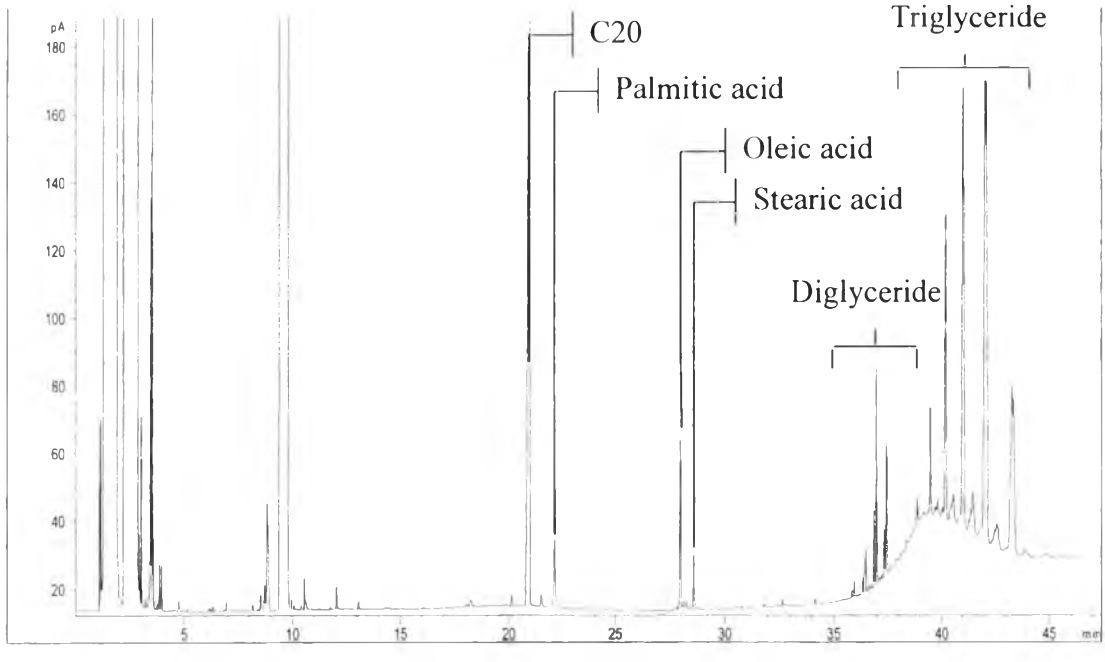

Figure 4.14 Chromatogram of 20 vol% beef oil in dodecane.

Table 4.7 Composition of beef fat feedstock

Component	Composition (wt. %)
Triglycerides	79.84
Diglycerides	10.60
Oleic acid	5.13
Palmitic acid	2.84
Stearic acid	1.59

Table 4.8 Fatty acid composition of beef fat*

Fatty Acid	Acronym	Formula	Beef Fat (wt. %)
Saturated Fat			47.20
Caprylic acid	8:0	$C_8H_{16}O_2$	0.02
Capric acid	10:0	$C_{10}H_{20}O_2$	0.05
Lauric acid	12:0	$C_{12}H_{24}O_2$	0.11
Myristic acid	14:0	$C_{14}H_{28}O_2$	3.3
	15:0	$C_{15}H_{30}O_2$	0.39
Palmitic acid	16:0	$C_{16}H_{32}O_2$	26.13
	17:0	$C_{17}H_{34}O_2$	0.67
Stearic acid	18:0	$C_{18}H_{36}O_2$	16.38
Arachidic acid	20:0	$C_{20}H_{40}O_2$	0.15
Behenic acid	22:0	$C_{22}H_{44}O_2$	-
Lignoceric acid	24:0	$C_{24}H_{48}O_2$	-
Unsaturated Fat			47.87
Monounsaturated Fatty Acid			46.50
Myristoleic acid	14:1	$C_{14}H_{26}O_2$	1.07
Palmitoleic acid	16:1	$C_{16}H_{30}O_2$	0.84
cis-9-Oleic acid	18:1	$C_{18}H_{34}O_2$	40.71
cis-11-Eicosenoic acid	20:1	$C_{20}H_{38}O_2$	0.88
Erueic acid	22:1	$C_{22}H_{42}O_2$	-
Nervonic acid	24:1	$C_{24}H_{46}O_2$	-
Polyunsaturated Fatty Acid			1.37
cis-9, 12-Linoleic acid	18:2	$C_{18}H_{32}O_2$	1.18
α-Linolenic acid	18:3	$C_{18}H_{30}O_2$	0.08
cis-11,14-Eicosadienoic acid	20:2	$C_{20}H_{36}O_2$	-
Arachidonic acid	20:4	$C_{20}H_{32}O_2$	-
cis-8,11,14-Eicosatrienoic acid	20:3	$C_{20}H_{34}O_2$	0.06
cis-8,14,17-Eicosatrienoic acid	20:3	$C_{20}H_{34}O_2$	0.05
4,7,10,13,16,19-Docasahexaenoic acid	22:6	$C_{22}H_{32}O_2$	-

*Data from Central Laboratory (Thailand) Co.,Ltd.

4.2.3 Effect of Catalyst Preparation on the Deoxygenation of Beef Fat over Pd Supported Titania Catalysts

A blank test for deoxygenation of triglyceride of beef fat was performed in the presence only commercial P-25 titania support at constant conditions under 500 psig, 325 °C, liquid hourly space velocity (LHSV) of 1 h^{-1}, and H_2/feed molar ratio of 30. The extent of thermal deoxygenation under these conditions was minor; the results showed that < 5 wt.% of triglycerides was converted. The main products formed were free fatty acid (palmitic acid, oleic acid, and stearic acid), heavy ester, and diglycerides as summarized in Table 4.9. The triglycerides of beef fat was hydrogenated and broken down into these various undesired products considered as the intermediates.

Heterogeneous catalytic triglyceride deoxygenation under the same constant temperature, reaction pressure, and H_2/feed molar ratio with the thermal deoxygenation was conducted via liquid hourly space velocity (LHSV) of 1 and 2 h^{-1} The results showed that beef fat can be converted to paraffinic hydrocarbons that have carbon atom in diesel specification range (C15 to C18 hydrocarbons). The major products from beef fat are n-heptadecane (n-C17) and n-pentadecane (n-C15), alkane products that have one carbon atom less than the original fatty acids in each oil molecule, indicate that the deoxygenation of beef fat over Pd/TiO_2 catalysts tends to undergo decarboxylation/decarbonylation pathway rather than hydrogenation pathway (Huber *et al.*, 2007, Snare *et al.*, 2006). The small difference can be noticed from the catalytic activity and selectivity on the deoxygenation of beef fat over 1 wt% Pd supported TiO_2 catalysts prepared by incipient wetness impregnation (IWI) using both SG-TiO_2 and P25-TiO_2 support (P25-IWI and SG-IWI catalysts). The above catalysts gave the average conversion of triglycerides about 90-100 % and 60-70 % in case of the selectivity to the desired products as summarized in Table 4.10.

As mentioned previously, there was only small difference of the catalytic activity and selectivity of the desired products between P25-IWI and SG-IWI catalysts in both liquid hourly space velocity (LHSV) of 1 and 2 h^{-1}. For a more extensive investigation, the deoxygenation of triglyceride of beef fat over palladium

supported titania catalysts under similar reaction condition as used in the previous was conducted via liquid hourly space velocity (LHSV) of 4 h^{-1}. 1 wt% Pd supported TiO_2 catalysts prepared by incipient wetness impregnation (IWI) and photochemical deposition (PCD) using both SG-TiO_2 and P25-TiO_2 support were carried out on the deoxygenation with the liquid hourly space velocity of 4 h^{-1}. Moreover, Pd/TiO_2 catalyst synthesized via a combined single-step sol-gel process (SSSG) with surfactant-assisted templating method (SATM) was conducted to compare with other methods. The prepared catalysts were tested for their catalytic activity and selectivity in deoxygenation of beef fat to hydrogenated biodiesel in a continuous flow fixed bed reactor at the same condition. The results showed that the beef fat can be converted to paraffinic hydrocarbons that have carbon atom in diesel specification range (C15 to C18 hydrocarbons) over all catalysts as shown in Figure. 4.15 – 4.19 and summarized in Table 4.6. The major products from beef fat are n-heptadecane (n-C17) and n-pentadecane (n-C15) as explained in case of LHSV of 1 and 2 h^{-1}.

1 wt.% Pd/TiO_2 catalyst synthesized via a combined single-step sol-gel process with SATM (SSSG) was successfully achieved with the higher activity and selectivity to the desired products. SSSG catalyst gave the average conversion of triglycerides about 80-90 %. Beside, SSSG catalyst was also an excellent catalyst for selective deoxygenation of beef fat to hydrocarbon in diesel specification range. The selectivity to diesel range hydrocarbon was very high, 80 %, while the selectivity to intermediates (palmitic acid, oleic acid, stearic acid, heavy esters, and diglycerides) was 12-14 %. From the result, it may cause by the highest surface area of SSSG catalyst (113 m^2g^{-1}) among other Pd/TiO_2 catalysts as shown in Table 4.1. Palladium ion tends to well disperse in mesopore of TiO_2 support during sol-gel process with surfactant-assisted templating method. The high surface area and high metal dispersion on the support of SSSG catalyst may result in the increased accessibility of reactant to the catalyst surface active sites existing along the mesoporous network.

P25-IWI catalyst gave the lowest average conversion of 20-40 %, as shown in Figure 4.14. The main products were n-heptadecane and n-pentadecane, resulting from decarboxylation/decarbonylation pathway. The desired product (hydrocarbon in diesel range, C15-C18) selectivity achieved almost 60 wt.%. In addition, the intermediates (palmitic acid, oleic acid, stearic acid, diglyceride and heavy ester)

were observed about 40-45 wt.%. The lowest conversion of triglyceride over Pd-IWI catalyst among other catalysts can be referred to the high coke deposition of 10.42 wt.% as shown in TPO results.

In comparative study between the effect of incipient wetness impregnation (IWI) and photochemical deposition (PCD) on the deoxygenation of beef fat for the production of hydrogenated biodiesel, the results showed that Pd/TiO_2 prepared by photochemical deposition method gave the higher conversion of triglycerides only in case of using P25-TiO_2 as the support. On the other hand, palladium supported SG-TiO_2 prepared by incipient wetness impregnation gave the higher conversion of triglycerides when compared to the one prepared via photochemical deposition. The overall results correspond to the palladium dispersion on the titania support in the following order: SG-IWI > SG-PCD > P25-PCD > P25-IWI.

In the effect of support, palladium loaded on SG-TiO_2 support via both incipient wetness impregnation (SG-IWI) and photochemical deposition (SG-PCD) gave the higher conversion of triglyceride (40-70 wt.%) and higher selectivity to the desired products (60-70 wt.%) as a result of the higher surface area of SG-TiO_2 support (89.6 m^2g^{-1}) compared to P25-TiO_2 support (50.5 m^2g^{-1}). The higher surface area provides the higher metal dispersion resulting in the larger the fraction of the metal atoms that are exposed at surfaces, where they are accessible to reactant molecules and available for catalysis (Zhang, *et al.* (2004)).

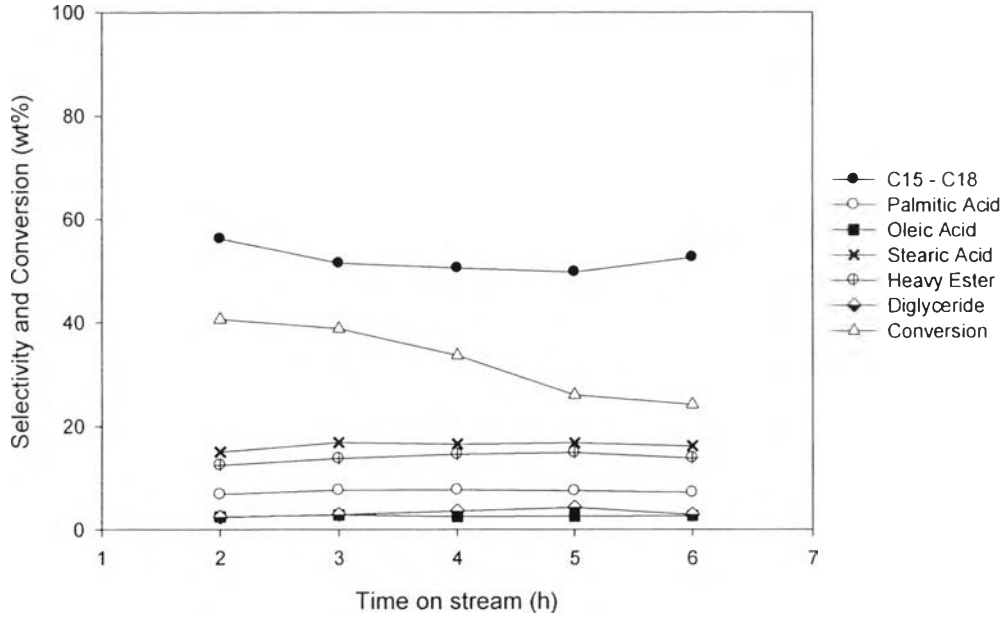

Figure 4.15 Conversion of triglyceride and selectivity as a function of time on stream of P25-IWI catalyst (reaction condition: 500 psig, 325 °C, LHSV of 4 h^{-1}, and H_2/feed molar ratio of 30).

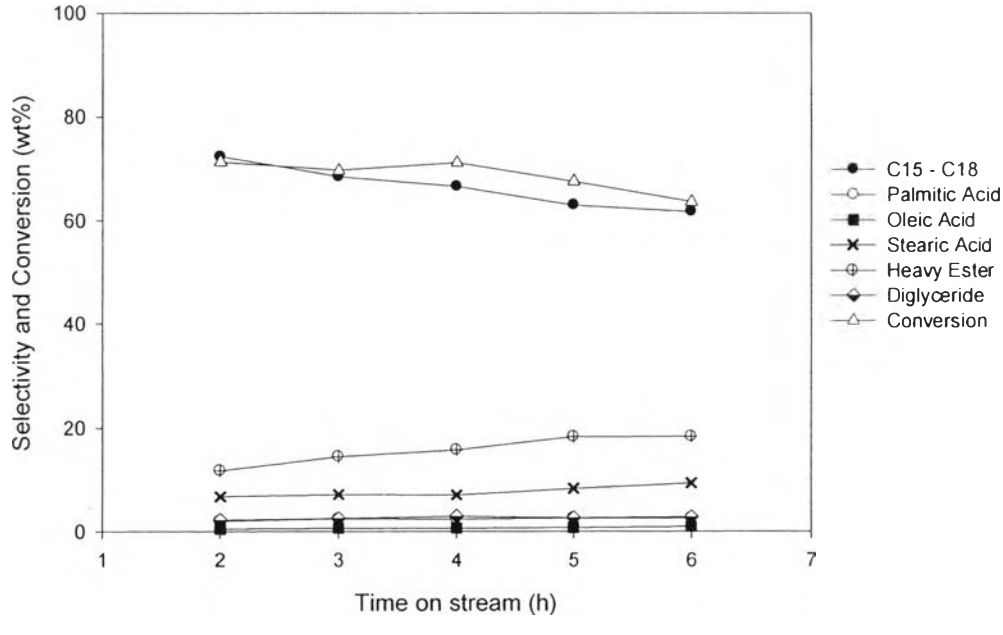

Figure 4.16 Conversion of triglyceride and selectivity as a function of time on stream of SG-IWI catalyst (reaction condition: 500 psig, 325 °C, LHSV of 4 h^{-1}, and H_2/feed molar ratio of 30).

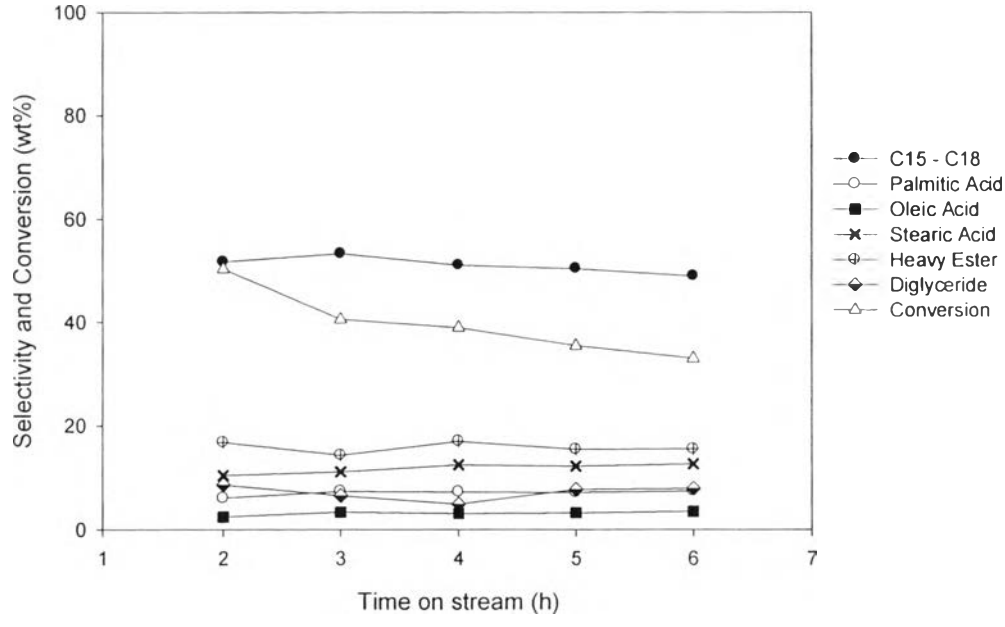

Figure 4.17 Conversion of triglyceride and selectivity as a function of time on stream of P25-PCD catalyst (reaction condition: 500 psig, 325 °C, LHSV of 4 h^{-1}, and H_2/feed molar ratio of 30).

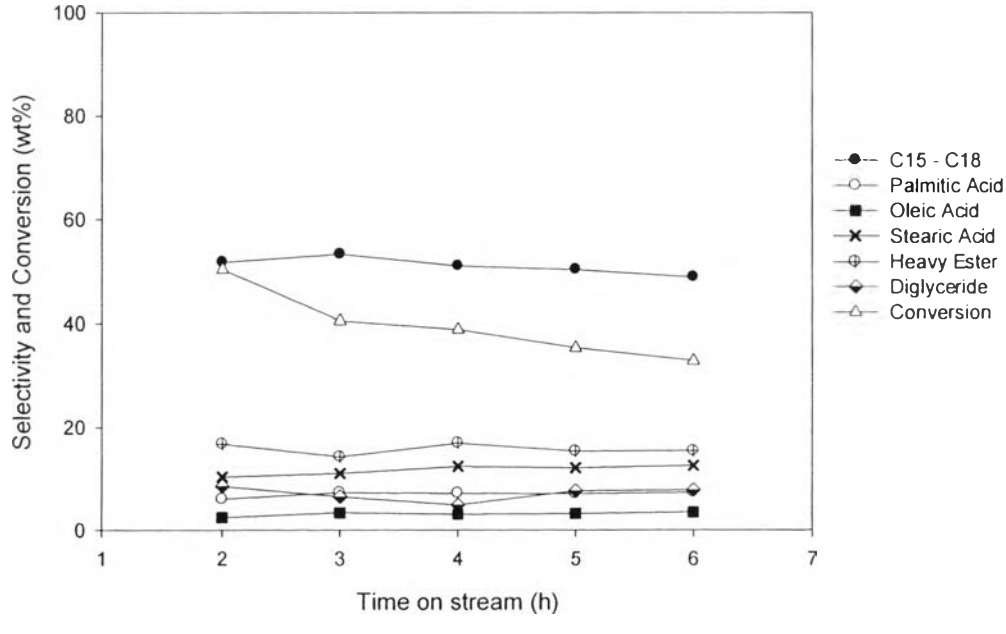

Figure 4.18 Conversion of triglyceride and selectivity as a function of time on stream of SG-PCD catalyst (reaction condition: 500 psig, 325 °C, LHSV of 4 h^{-1}, and H_2/feed molar ratio of 30).

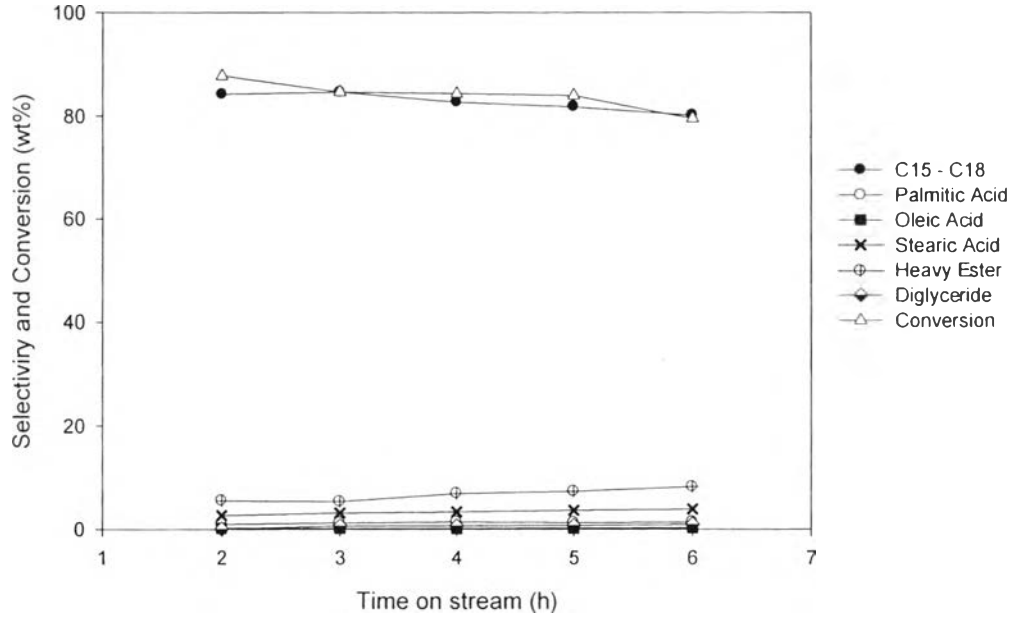

Figure 4.19 Conversion of triglyceride and selectivity as a function of time on stream of SSSG catalyst (reaction condition: 500 psig, 325 °C, LHSV of 4 h^{-1}, and H_2/feed molar ratio of 30).

Table 4.9 Product distribution on the deoxygenation of beef fat over Pd/TiO_2 catalysts.

Catalyst	P25-TiO_2 (Blank)		P25-IWI				SG-IWI			
LHSV (h^{-1})	1		1		2		1		2	
Time on stream (h)	4	6	4	6	4	6	4	6	4	6
Conversion of Triglyceride	4.61	4.96	97.01	96.94	89.64	87.80	98.07	97.96	94.86	94.78
Selectivity										
Total C15-C18	-	-	69.27	66.19	68.63	64.49	65.42	63.85	64.73	61.98
n-C15	-	-	17.25	17.06	16.99	15.65	17.45	15.67	17.00	16.61
n-C16	-	-	5.86	5.28	5.54	5.52	3.92	4.31	4.81	4.70
n-C17	-	-	37.19	35.74	36.67	33.97	37.88	36.84	35.67	33.81
n-C18	-	-	8.97	8.11	9.43	9.35	6.17	7.03	7.25	6.86
(C15+C17)/(C16+C18)	-	-	3.67	3.94	3.58	3.33	5.48	4.63	4.37	4.36
Intermediates	100	100	26.14	29.79	27.97	32.30	31.24	33.04	31.28	34.07
Palmitic acid	19.77	20.07	5.13	5.11	2.77	3.33	4.83	4.78	2.18	2.88
Oleic acid	22.57	21.61	-	-	-	-	-	-	-	-
Stearic acid	12.69	13.00	9.55	9.85	5.91	7.22	10.15	10.02	8.59	9.63
Ester	14.43	13.73	9.18	11.99	17.01	19.63	14.18	15.57	18.22	19.23
Diglyceride	30.54	31.59	2.28	2.84	2.28	2.12	2.08	2.67	2.29	2.33
Others	-	-	4.59	4.02	3.40	3.21	3.34	3.11	3.99	3.95
n-C13	-	-	3.40	2.95	2.32	2.14	2.51	2.24	2.91	2.58
n-C14	-	-	1.19	1.07	1.08	1.07	0.83	0.87	1.08	1.37

*Reaction condition: 500 psig, 325 °C, and H_2/feed molar ratio of 30

Table 4.10 Product distribution on the deoxygenation of beef fat over Pd/TiO_2 catalysts.

Catalyst	P25-IWI		SG-IWI		P25-PCD		SG-PCD		SSSG	
Time on stream (h)	4	6	4	6	4	6	4	6	4	6
Conversion of Triglycerides	33.70	24.24	71.11	63.56	38.92	32.96	41.57	41.01	84.34	79.51
Selectivity										
Total C15-C18	50.50	52.59	66.52	61.66	51.03	48.89	57.88	54.88	82.68	80.17
n-C15	11.17	12.53	13.86	11.56	10.29	12.67	13.08	11.97	20.54	19.82
n-C16	5.31	4.69	8.77	8.64	5.81	4.91	6.70	7.07	6.88	7.23
n-C17	24.46	27.05	28.75	25.49	24.89	22.68	26.49	23.66	43.56	41.19
n-C18	9.56	8.32	15.14	15.97	10.04	8.63	11.61	12.18	11.70	11.93
(C15+C17)/(C16+C18)	2.40	3.04	1.78	1.49	2.22	2.61	2.16	1.85	3.45	3.18
Intermediates	45.05	42.89	28.89	34.20	44.60	46.93	38.92	41.80	12.54	14.63
Palmitic acid	7.70	7.22	2.37	2.56	7.25	7.40	5.09	4.07	1.42	1.36
Oleic acid	2.51	2.65	0.63	0.94	3.08	3.52	2.22	2.61	0.17	0.27
Stearic acid	16.59	16.22	7.13	9.48	12.42	12.63	9.31	10.69	3.37	3.89
Ester	14.65	13.90	15.82	18.40	16.99	15.50	16.76	17.67	6.91	8.19
Diglyceride	3.60	2.90	2.94	2.82	4.86	7.88	5.54	6.76	0.67	0.92
Others	4.45	4.52	4.59	4.14	4.37	4.18	3.20	3.32	4.78	5.20
n-C13	3.39	3.55	2.92	2.57	3.23	3.21	1.98	2.02	3.47	3.79
n-C14	1.06	0.97	1.67	1.57	1.14	0.97	1.22	1.30	1.31	1.41

*Reaction condition: 500 psig, 325 °C, LHSV of 4 h^{-1}, and H_2/feed molar ratio of 30